Research Article
Open Access

MJ Cell Press

MJ Engineering Sciences

Available at: https://mjcellpress.com/article/mjes03/

MJ Engineering Sciences

Enhanced wind turbine blade design for improved power output and reduced noise

Gnepie-Takam Nicolas[1], Choupo Yuego[1], Tientcheu-Nsiewe Max-well[1], Matuam Tamdem Balbine[1], et Kuitche Alexis[1]

[1]Laboratory of Applied Energy and Thermal Science (LETA), National Higher School of Agro-industrial Sciences-Ngaoundere, Cameroon

[*]Corresponding author: gnepienicolas@gmail.com

Key words

Wind Turbine,
Optimization,
Vortex method,
Aerodynamic performance.

Abstract

Current wind turbine optimization studies primarily employ either the Blade Element Method (BEM) or Computational Fluid Dynamics (CFD) to evaluate rotor aerodynamic performance. While BEM remains widely used due to its simplicity and low computational cost, it depends heavily on empirical correction factors that can limit its accuracy in complex flow conditions. Conversely, although CFD provides highly accurate results by solving the Navier-Stokes equations, it is computationally expensive and often impractical for large-scale parametric studies. Vortex methods—particularly the prescribed wake method—offer a promising compromise, balancing computational efficiency with acceptable levels of accuracy. In the present study, we propose a novel wind turbine blade model derived through a multi-objective optimization of the blade's geometric parameters, specifically chord distribution and twist angle. The aerodynamic performance of the optimized blade is evaluated using an enhanced prescribed wake model. Aerodynamic noise is estimated using Brooks' empirical method, while the blade production cost is calculated using Zudong's cost model. The resulting blade design demonstrates a 3% increase in power output, a 0.02 dB reduction in noise emissions, and a marginal 1.2% increase in production cost. These findings suggest that moderate improvements in performance and environmental impact can be achieved through geometry-based optimization without substantial cost penalties.

Received:17.03.2025 Accepted: 23.05.2025 Published online: 25.06.2025

How to cite this article: Gnepie-Takam N., Choupo Yuego, Tientcheu-Nsiewe M., Matuam Tamdem B., & Kuitche A. (2025). *Enhanced Wind Turbine Blade Design for Improved Power Output and Reduced Noise. MJ Engineering Sciences,1*(1), 31–48. https://doi.org/10.63156/mjes03.

1. Introduction

Being able to compete with the cost of traditional fossil fuel sources remains one of the major challenges faced by the global wind turbine industry. In response to this challenge, wind turbines have evolved into massive rotating machines with a wide range of blade shapes. In the pursuit of optimal blade geometries, stochastic optimization algorithms have been widely adopted by the industry and thoroughly investigated in the literature. Whether single-objective or multi-objective optimization is conducted, the aerodynamic performance function consistently appears as a key component ([1], [2], [3], [4], [5]).

Typically, aerodynamic performance is evaluated using the Blade Element Momentum (BEM) method, which is widely adopted due to its rapid convergence ([6], [7]). However, the basic formulation of BEM has several limitations. First, it relies on multiple correction parameters, which reduces its accuracy. Furthermore, the downstream flow structure is simplified as a cylindrical tube with a radius R equal to that of the wind turbine. The critical challenge in assessing aerodynamic performance lies in accurately estimating the velocity fields and the angle of incidence. Aerodynamic forces depend on these two parameters, which in turn are influenced by the induced velocities resulting from the shape of the downstream wind structure—also referred to as the wake [8]. Variations in the wake structure lead to corresponding variations in induced velocity, followed by changes in relative velocity and the local angle of incidence, which ultimately affect the aerodynamic load on the rotor. Hence, it is crucial to account for the actual structure of the wake. An experiment conducted by the NREL laboratory on a single-blade wind turbine equipped with a blade tip smoke generator revealed that the downstream wake is dominated by marginal vortices originating from the blade tip. However, in BEM, the downstream wake is simplified to a cylindrical tube, which impacts the estimation of induced velocities, relative velocity, angle of incidence, and consequently, the resulting aerodynamic forces.

In addition to BEM, other aerodynamic modeling methods include vortex methods and Navier-Stokes equation resolution techniques. While Navier-Stokes methods offer greater accuracy, they remain computationally prohibitive, even with the use of Hakani's method, which seeks to reduce computation time [9]. Vortex methods are potential flow approaches that replace the real flow through the rotor with an equivalent vortex system [10]. These systems consist of blade-bound vortices, free vortex sheets shed from the blades, and tip vortices [11]. Among the vortex-based approaches, the prescribed wake method offers a better trade-off between computational cost and accuracy [12]. In this method, the downstream wake is assumed to be known from approximate calculations. The wake can be modeled using concentric circles, helicoids, or rigid vortex segments ([13], [14], [15]). Meglaoui [12] demonstrates that concentric circles are preferable for wake modeling. Choupo [16] refined the method by incorporating vortex growth phenomena, improving its accuracy by approximately 5%.

This study aims to design a blade that balances power output, acoustic performance, and production cost. To achieve this, the Particle Swarm Optimization algorithm is coupled with the modified prescribed wake method to evaluate aerodynamic performance, Brooks' method [17] to estimate aerodynamic noise, and Zudong's method [18] to assess production cost.

2. Material et methods

2.1. Material

The physical model used in this study is the NREL PHASE IV two-bladed wind turbine with profile S809 airfiole profile. The rotor characteristics are summarized in Table 1 [19].

Table 1 : Geometric characteristics of the rotor

r_{da}(m)	r_{fa}(m)	N	Θ[°]	Ω[tr/mn]	D[m]	Blade profile
1,2573	4,903	2	3°	71,63	10	twisted S809 airfoil

The evolution of the chord and twist along the blade are given in tables 2 and 3.

Table 2 : Evolution of chord

r[m]	1,083	1,163	1,284	1,385	1,586	1,747	1,928	2,119	2,290	2,431	2,602
c[m]	0,716	0,7049	0,6914	0,679	0,679	0,648	0,631	0,616	0,604	0,590	0,575

Table 3 : Evolution of twist

r[m]	1,083	1,123	1,163	1,243	1,323	1,443	1,572	1,722	1,892	2,061	2,241	2,380
b[°]	17,20	16,38	15,48	14,12	12,85	11,40	10,13	8,862	7,682	6,682	5,592	4,865

2.2. Methods

2.2.1. Optimization method: Particle swarm optimization algorithm

Introduced by Eberhart and Kennedy [20], these algorithms are inspired by the coordinated movement of insect swarms and bird flocks. The Particle Swarm Optimization (PSO) algorithm searches for solutions to optimization problems by imitating how birds and insects move collectively to find food or avoid predators. The individuals in the algorithm are called particles, and the population is referred to as a swarm. Thus, a swarm of particles represents potential solutions to the problem.

The velocity and position of each particle are given by equations (1) and (2) respectively:

$$vit_{ij}(t+1) = wvit_{ij}(t) + C_1 r_1 \left(pos_{besti} - vit_{ij}(t)\right) + C_2 r_2 \left(pos_{best} - vit_{ij}(t)\right) \quad (1)$$

$$pos_{ij}(t+1) = pos_{ij}(t) + vit_{ij}(t+1) \quad (2)$$

Where:

C_1, C_2: Acceleration coefficients

w: Inertia factor (values assigned based on [21])

pos_{besti}: The best position of particle *i* in the population

pos_{best}: The best position in the entire population

The flowchart of the method is given in Figure 1

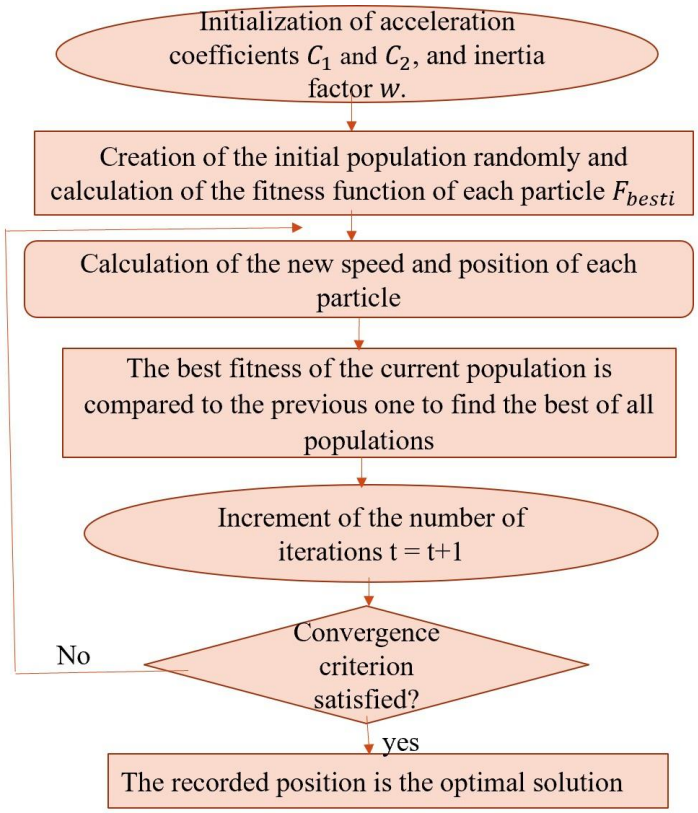

Figure 1: Flowchart of the PSO method [22].

2.2.2. Objective functions

For this study, we opted for a multi-objective optimization approach which can be formally described as follows:

$$\begin{cases} \text{Minimize } f(x) = \big(f_1(x), f_2(x), \dots, f_k(x)\big), (k \text{ the number of objectives}) \\ \text{under constraints } C_i(x) \text{ with } i \text{ ranging from1 à } m \ (m \text{ he number of constraints}) \\ \text{with } x \in X \end{cases}$$

The resolution method used is the weighting approach which involves assigning a weight to each objective function a. Thus, the optimization problem is transformed into a single-objective problem:

$$\begin{cases} \text{Minimize } f(x) = \big(a_1 f_1(x) + a_2 f_2(x) + \cdots + a_k f_k(x)\big), (k \text{ the number of objectives}) \\ \text{under constraints } C_i(x) \text{ with } i \text{ ranging from1 à } m \ (m \text{ he number of constraints}) \\ \text{with } x \in X \end{cases}$$

The chosen objective functions for this study are:

- Maximizing aerodynamic performance, in other words, the primary goal is to maximize the useful power (P), or to minimize (1/P).

- Reducing production costs to make the wind energy more competitive in the market.

- Minimizing aerodynamic noise, the noise pollution is one of the main disadvantages of wind turbines.

2.2.2.1. Power assessment model

The useful power is evaluated using the modified prescribed wake method proposed by Choupo [16]. This method provides a more accurate estimation of airflow behind the turbine compared to BEM. The wake downstream of the wind turbine is modeled as shown in figure (2). The wake-induced velocities downstream of the rotor are expressed by the following equations (3) and (4)

$$V_r(r,z) = v = \left(-\Gamma/2\pi\sqrt{z^2+(r+R_w)^2}\right)\left(K(s) + \left({R_w}^2 - r^2 - z^2/z^2 + (R_w - r)^2\right)E(s)\right) \quad (3)$$

$$V_z(r,z) = u = \left(-\Gamma/2\pi\sqrt{z^2+(r+R_w)^2}\right)\left(K(s) - \left({R_w}^2 + r^2 + z^2/z^2 + (R_w - r)^2\right)E(s)\right) \quad (4)$$

Where:

$$R_w(z) = (105C_1^2/2\pi)^{1/5}\left(C_T\Omega(z+z_0)\right)^{1/3} \quad (5)$$

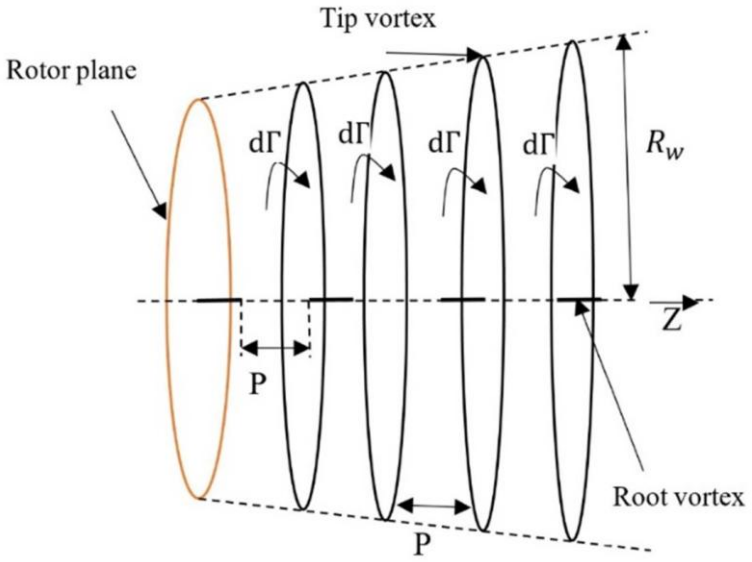

Figure 2: Structure of the wake downstream of the wind turbine [16]

2.2.2.2. Cost model evaluation

The rotor (hub + blade assembly) accounts for approximately 22.3% of the total cost of the wind turbine. A well-designed rotor with high aerodynamic efficiency is essential for achieving low energy costs. For this reason, the cost function is often limited to the rotor ([18], [23]). This is defined by:

$$C\_rotor = b\_rotor + (1 - b\_rotor)\, w\_rotor \quad (6)$$

Where:

b_rotor, represents fixed costs such as : transportation, installation and operating expenses.

b_rotor=0,1 as recommended by Xudong [18]

w_rotor represents variable costs such as: the cost of materials, design procedure and labor.

w_rotor is derived from the relative material usage, given by equation (7)

$$w_{rotor} = \sum_{i=1}^{N} \frac{m_i c_i}{M_{tot} c_{i,or}} \quad (7)$$

Where:

m_i : mass of the i-th element of the blade

c_i : average chord of the i-th blade element

M_{tot}: total mass of the original blade geometry

$c_{i,or}$: mean chord of the i-th element of the original blade geometry

N: total number of blade elements

The mean chord of the blade element is the average value of two chords: the "root" and "tip" sides of the element.

2.2.2.3. Noise model

Among the semi-empirical models, Brooks' (1989) model is one of the most validated for predicting aerodynamic noise in wind turbines [17]; they conducted a sophisticated validation study of their noise emission model against three independent measurements made at the United Technologies Research Center (UTRC) by Schlinker and Amiet.

According to Brooks [17] the noise made by wind turbines has 6 sources, according to Lowson [24], but most significant sectors are the turbulent flow noise and the profile noise. In this study, we will only consider these two sectors and the Brooks' (1989) model will be used to model them:

2.2.2.3.1. Turbulent flow noise

Wind turbine noise can be broken-down into a range of frequencies emitted by each turbine, which affects the overall ground noise. The breakdown of turbulence noise into range of frequencies, gives turbulence noise which can be expressed as the root mean square of its frequency components, as follows: $SPL_{fn} = \sqrt{\sum_F SPL_f}$; where F represents the frequency range considered.

The octave band frequency range corresponds to the study of aerodynamic noise which is A band.

F= {63, 125, 250, 500, 1000, 2000, 4000, 8000} Hz. The unit of sound pressure level is given in dB(A).

The noise level for each frequency range is determined with the equation (8)

$$SPL_f = 58.4 + 10log\left[\rho^2 c_0^2 l M^3 I^2 k^3 L\,(1+k^2)^{7/3}/r^2\right] + 10log\left(\frac{LFC}{1+LFC}\right) \quad (8)$$

Where:

L: length of the free stream turbulent flow

I: intensity of turbulence

k: wave number of the blade cross-section

Calculated as:

$$k = {}^{\pi f c_{av}}/_{V_{rel}} \quad (9)$$

c_{av} : mean chord of the blade element

V_{rel}: the relative wind speed of the blade element

c_0 : the speed of sound in air for standard ambient conditions assumed to be constant and is 340m/s

LFC : the low frequency correction factor defined as follows:

$$LFC = 10 \times S^2 k^2\, M/q^2 \quad (10)$$

S^2 is the Sears function squared is defined as:

$$S^2 = \left(\frac{2\pi k}{q^2} + \frac{1}{1+2{,}4k/q^2}\right)^{-1} \quad (11)$$

And

$$q^2 = 1 - M^2 \quad (12)$$

With

$$M = {}^{V_{rel}}/_{c_0} \quad (13)$$

The sound pressure level is calculated by equation (14) for the frequency range F and the entire blade is summarized with the interference law:

$$SPL_T = 10log(\sum_{i=1}^{N} 10^{0.1SPL_{fn}}) \quad (14)$$

Where:

N: the total number of elements

L: the turbulent flow length

I: turbulence intensity value, used for the equation which is assigned to considered free wind speed class, defined with the designer's initial information. According to the IEC standard (IEC61400-1,2005), there are four wind speed classes and two subclasses: A and B. for example, the designer can introduce wind speed class IIIA, which is related to the turbulent flow length, L=150m, and a turbulence intensity I=0.18

2.2.2.3.2. Natural noise of the profile

The natural noise of the blade profile has several subcomponents. In this study, the most significant sources of noise are considered: trailing edge noise and stall noise [3].

Trailing edge noise

Trailing edge noise is emitted due to the interaction of naturally turbulent flow passing over both the positive and negative pressure sides of the trailing edge of the airfoil. This flow transforms into a vortex, creating noise. For a blade element, the total noise is the sum of the noise on the intrados and extrados (equation 15)

$$SPL_T = 10log(10^{0.1SPL_D} + 10^{0.1SPL_S}) \quad (15)$$

Where:

SPL_D is the noise on the extrados in depression, calculated as:

$$SPL_D = 10log\left(\frac{M^5 \delta_p^* \bar{D}_h L}{r_e^2}\right) + A\left(\frac{St_P}{St_1}\right) + (K_1 - 3) + \Delta K_1 \quad (16)$$

And SPL_S the noise on the intrados in overpressure is calculated as:

$$SPL_S = 10log\left(\frac{M^5 \delta_S^* \bar{D}_h L}{r_e^2}\right) + A\left(\frac{St_s}{St_1}\right) + (K_1 - 3) \quad (17)$$

Where:

$St_{P,S} = f\,\delta_{p,s}^*/V$: Strouhal number for sunction and pression sides (18)

$\bar{D}_h$: is the directivity function for an observer located at the wind turbine; equal to 1;

δ^*: is the thickness of the boundary layer displacement which is determined with the Reynolds number;

$K_1, \Delta K_1, A$: are constants, is the St_1 Strouhal number defined in Brooks' model [17];

M: is the Mach number for the blade element;

r_e: the distance between the trailing edge noise source and the receiver, equal to the blade span distance, since noise emission studies are performed for the center of rotation at the receiver point.

Stall noise

When the angle of attack is relatively large, the boundary layer is peeled off over a large portion of the sunction surface, the size of the turbulent flow becomes larger, and over the entire suction surface the flow becomes unstable which generate stall noise. The sound pressure level of stall noise is given by:

$$SPL_{\alpha} = 10log\left(\frac{M^5 \delta_s^* \bar{D}_h L}{r_e^2}\right) + B\left(\frac{St_s}{St_2}\right) + K_2 \quad (19)$$

K_1, B are constants,

St_2 is the Strouhal number defined in Brook's model [18].

2.2.3. Estimation of the cost of kWh

Once the new blade model was proposed, a comparative analysis of the cost of kWh produced by the two blade models (basic blade model and optimized blade) was made. According to Sathyajith [25], there are several parameters in the estimation of the cost of wind power, including the location (wind speed, land cost, installation charges) and turbine parameters.

There are several methods of estimating the cost of kWh in the literature, the most widespread of which is the present cost value (PCV) method, which will also be used in this study. The PCV is given by equation (20).

$$PCV = 1 + C_{omr} \times \left[\frac{1+i}{r-i}\right] \times \left[1 - \left(\frac{1+i}{1+r}\right)^t\right] - S \times \left(\frac{1+i}{1+r}\right)^t \quad (20)$$

Where:

I: is the interest rate and is equal to 8%;

r: the inflation rate and is worth 6%;

t: The life of the machine is 20 years;

S: additional costs (including the cost of civil engineering, transportation of the turbine and road construction).S is assumed to be equal to 10% of the price of the wind turbine;

$C_{omr:}$ operating, maintenance and repair costs. Although varying depends on the years, it is generally estimated to vary between 15 to 30% of the total investment cost plus other costs in this study it is assumed to be 25% of the investment cost I.

Investment (I) is the sum of the price of the wind turbine and other initial costs, including infrastructure, installation and grid integration. These are estimated to be 20% of the turbine price.

The cost of the specific turbine depends on the rated power of the wind rotor, and also varies between manufacturers. It is summarized in the following table 4.

Table 4: Production cost of wind turbines [26]

Wind power (kW)	Specific cost ($/kW)	Average cost ($/kW)
<20	2200-3000	2600
20 – 200	1250-2300	1775
>200	700-1600	1150

Once the PCV is found the price of the kWh is given to us by equation 21

$$UCE(\$/kWh) = \frac{PCV}{AEP} \quad (21)$$

With

$$AEP = 8760 \int_0^{\infty} P(V) f(V) dV \quad (22)$$

$$P(V) = \left(\frac{k}{c'}\right)\left(\frac{V}{c'}\right)^{k-1} exp\left[-\left(\frac{V}{c'}\right)^{k}\right] \quad (23)$$

3. Results and discussion

Studies were conducted on the baseline blade to estimate its noise emissions and production cost.

3.1. Estimation of aerodynamic noise

The aerodynamic noise emitted by the NREL PHASE VI two-bladed rotor was evaluated using Brooks' method [17], for frequencies ranging from 100 to 1000 Hertz, as presented in Figure 3. It was observed that the noise level decreases with frequency, with the highest noise occurring at 150 Hertz. The main discrepancy between the experimental and simulated data is likely due to the exclusion of certain noise sources in the simulation. At 150 Hz, the noise along the blade was evaluated, as shown in Figure 4. From this figure, we observe that the noise level increases with the radius *r*. This is explained by the fact that, at the blade tip, the flow becomes more turbulent; indeed, the relative velocity increases with radius.

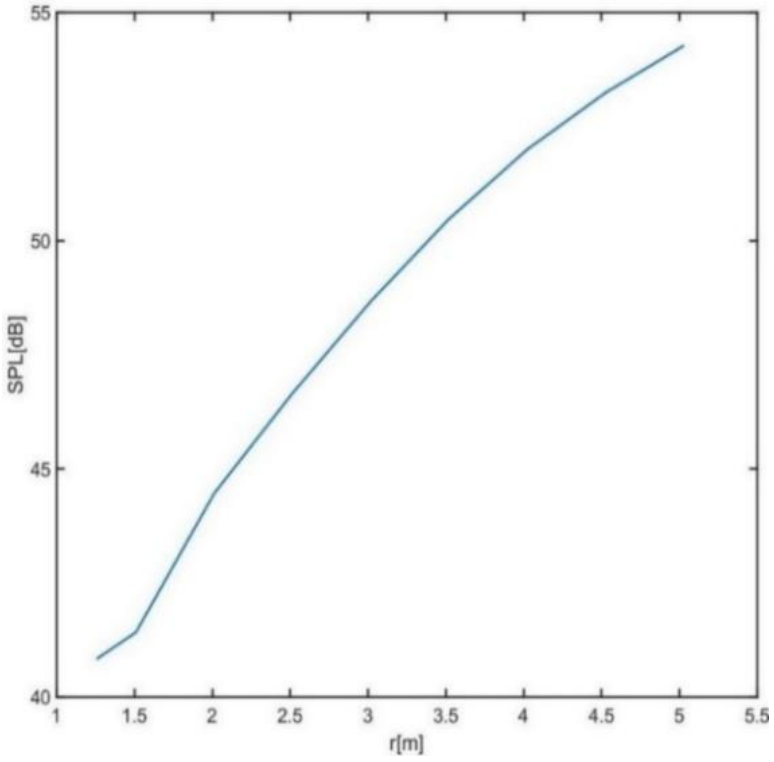

Figure 4: Evolution of the noise emitted along the blade for f=150Hz.

3.2. Cost estimation

Figure 5 shows the evolution of the production cost along the blade obtained by the Xudong's method [18].

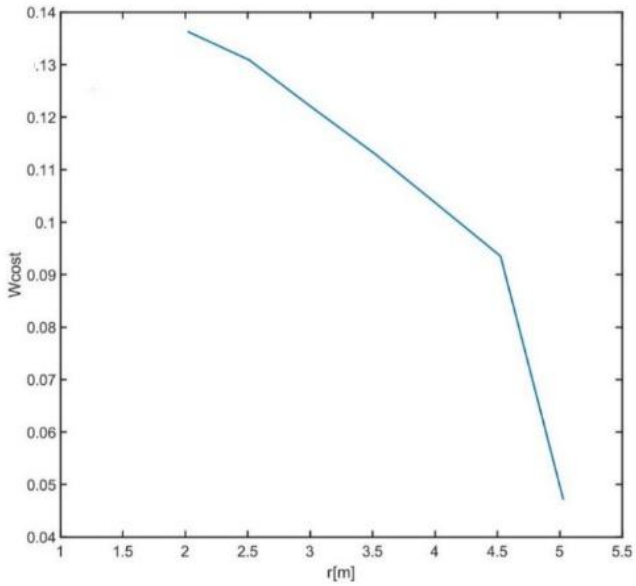

Figure 5: Evolution of production cost along the blade

It is observed that the cost of the blade decreases with the radius r. the total cost of the blade C_{rotor} is 1.

3.3. Optimization results

To carry out this optimization, 9 control points were selected as defined by Table 5: the control points assigned are radius, chord, twist and mass.

Table 5: Control points on the blade

Radius [m]	1,257	1,509	2,016	2,512	3,018	3,502	4,023	4,526	5,029
Chord[m]	0,697	0,6701	0,6243	0,5799	0,5339	0,4875	0,4436	0,3993	0,3582
Twist[rad]	0,3018	0,2702	0,2249	0,1961	0,1744	0,1574	0,1435	0,132	0,1263
Mass[kg]	5	5,1096	5,428	5,2112	4,848	4,4984	4,1128	3,7224	1,87552

3.3.1. Definition of the displacement domain

The optimization constraints considered were the chord and the twist. The domain of these design variables was defined by lower and upper limits as shown in Figures 6 and 7.

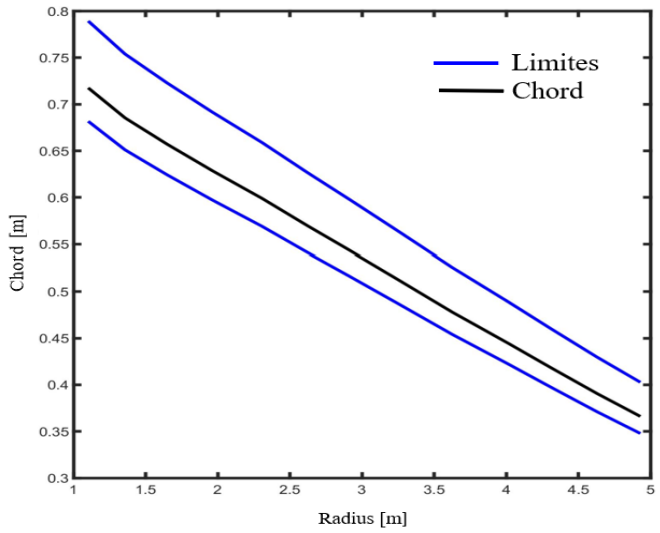

Figure 6: Lower and upper limits of the chord

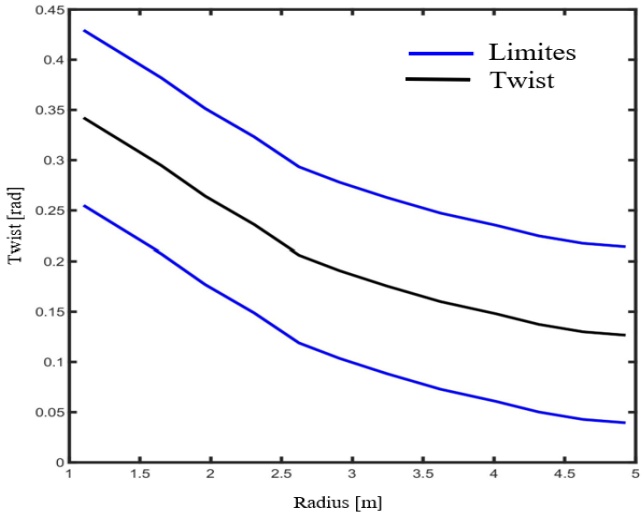

Figure 7: Lower and upper limits of the twist

The upper and lower limits of the design variables were parameterized using Matlab code (Figures 8 to 11). Each figure shows the parameterization equation and the error residuals at each control point. The lower limit and upper limit of the rope are parametrized respectively by linear equations of negative slope with a maximum residual of 0.05. And the lower limit and upper limit of the twist are parametrized by a polynomial of degree five with a maximum error of 0.001.

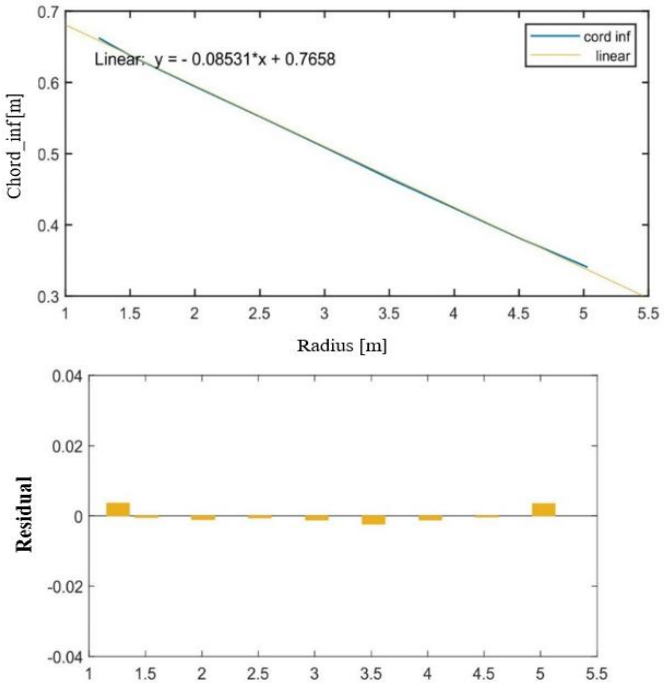

Figure 8: Parameterization of the lower limit of chord

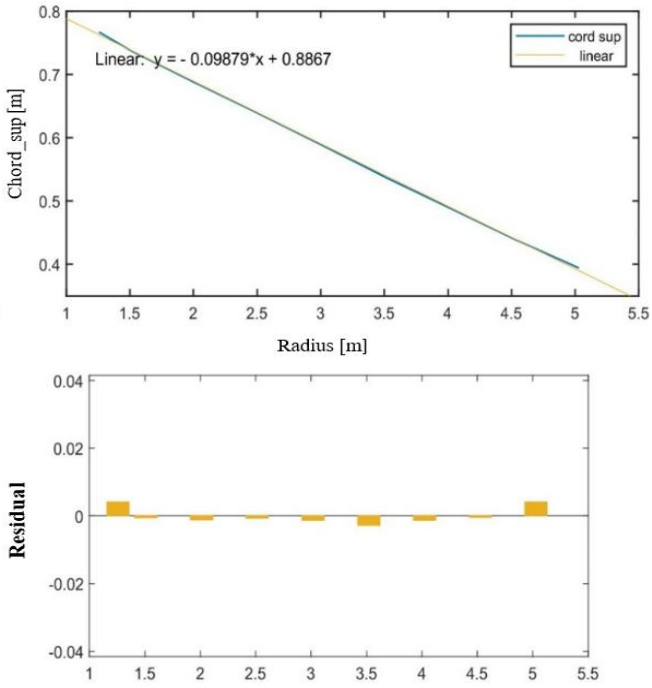

Figure 9: Parameterization of the upper limit of chord

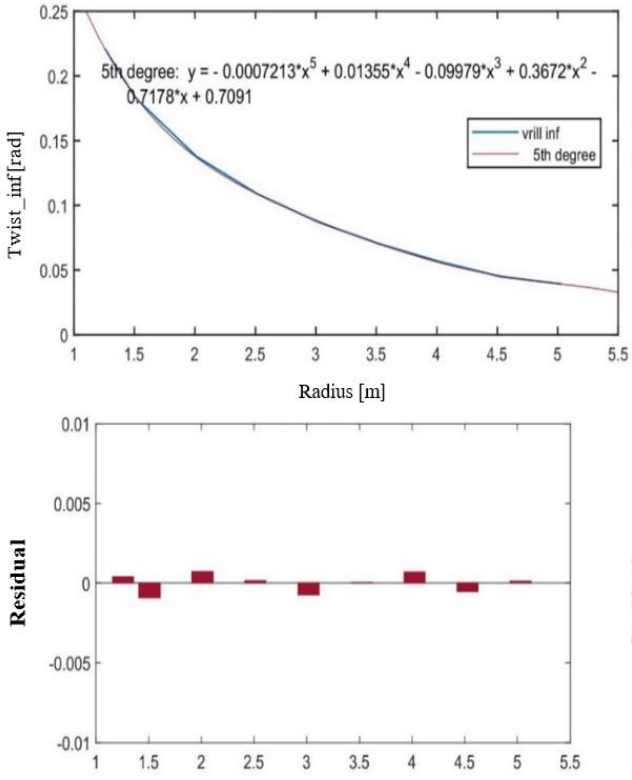

Figure 10: Parameterization of the lower limit of twist

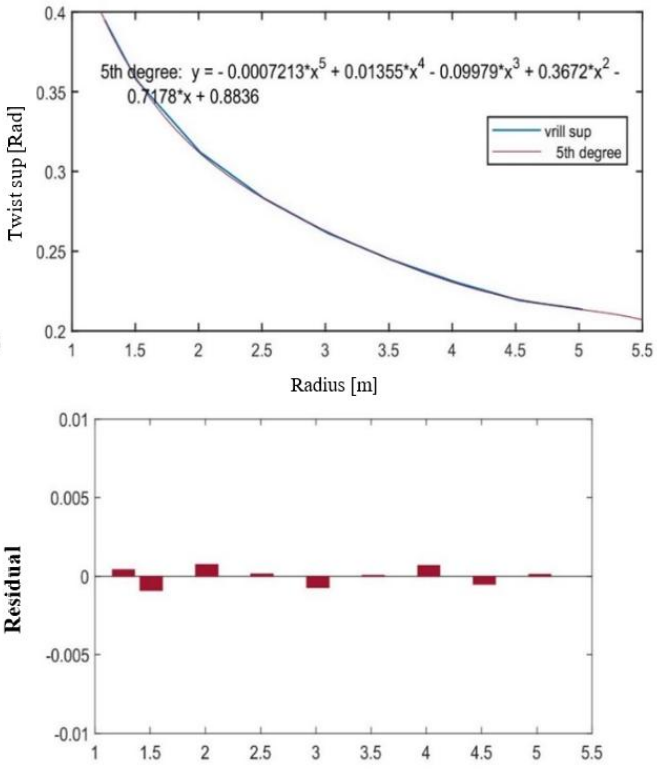

Figure 11: Parameterization of the upper limit of chord.

3.3.2. Parameters of the optimization algorithm

Several tests were conducted to determine the number of particles and iterations required to explore the domain and retain the optimal position. It was concluded that 100 particles and 150 iterations are needed for good convergence.

The value of inertia w is given by equation 26 and $C_2 = C_1 = 1{,}2$;

$$w = (0{,}9 - 0{,}5)/(1500 - i_{eme_{iter}}) \quad (26)$$

Each of these coefficients is multiplied by the rand function in MATLAB to preserve the probabilistic nature of the method and avoid getting trapped in local minima. The rand function randomly generates numbers between zero and one. The optimization was performed for a wind speed of 10 m/s, which is the nominal speed, and a frequency of 150 Hertz, which corresponds to the frequency where noise is most significant.

Figures 12 to 18 show the rope convergence and twist for the first, fourth and eighth control points respectively

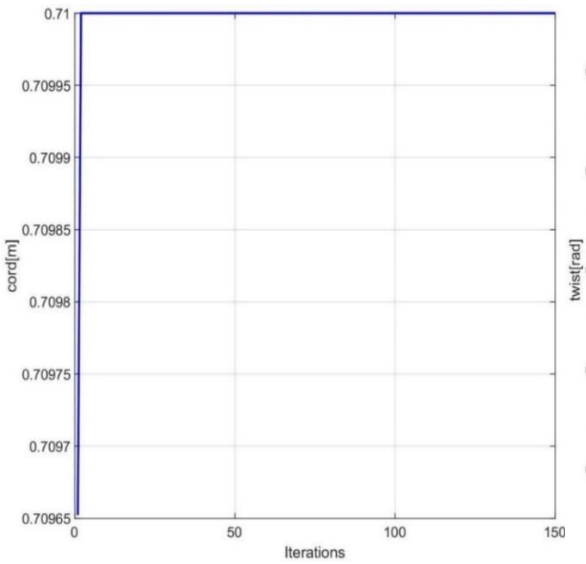

Figure 12: Convergence of the chord for the first control point

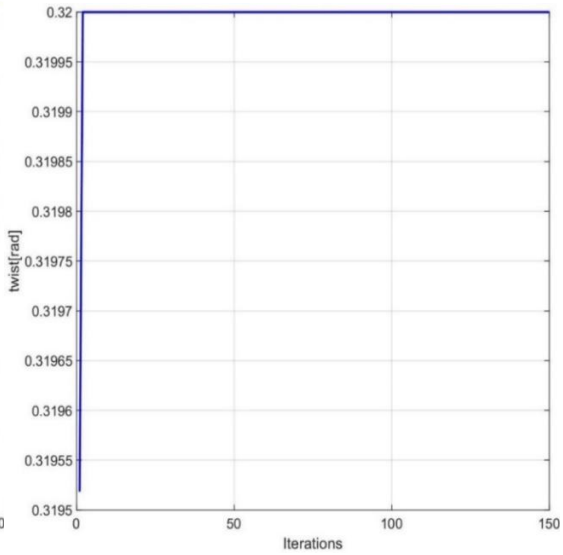

Figure 13: Convergence of the twist for the first control point

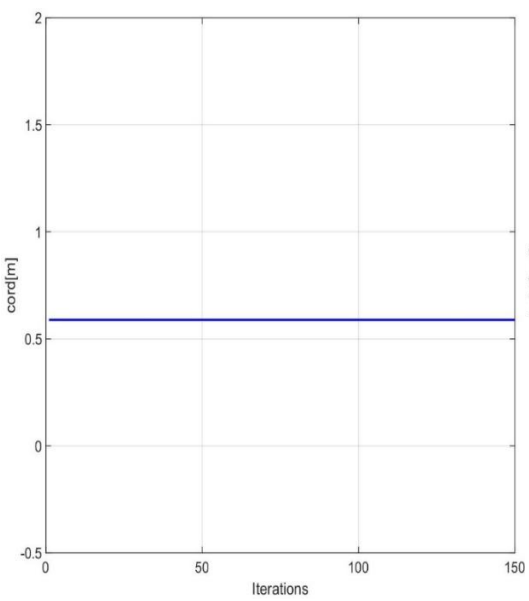

Figure 14: Convergence of the chord for the fourth control point

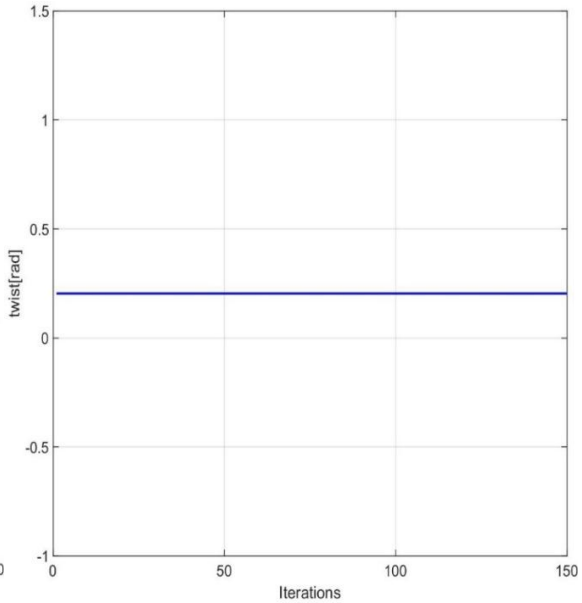

Figure 15: Convergence of the twist for the fourth control point

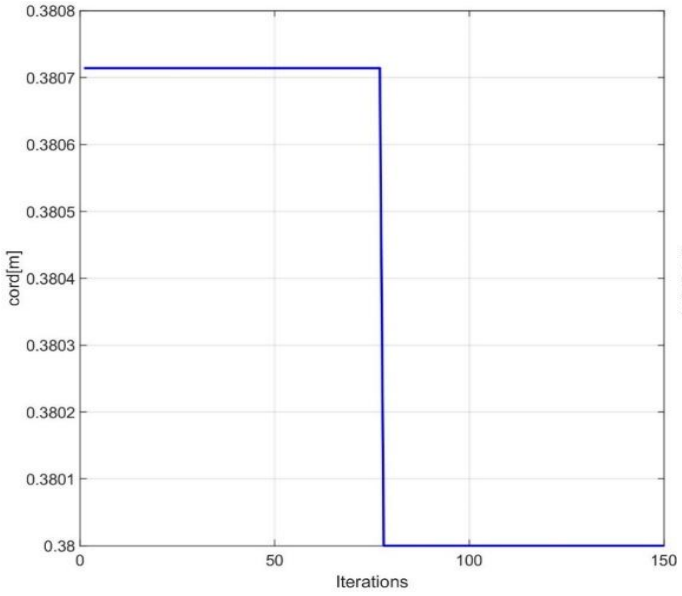

Figure 16: Convergence of the chord for the eighth control point

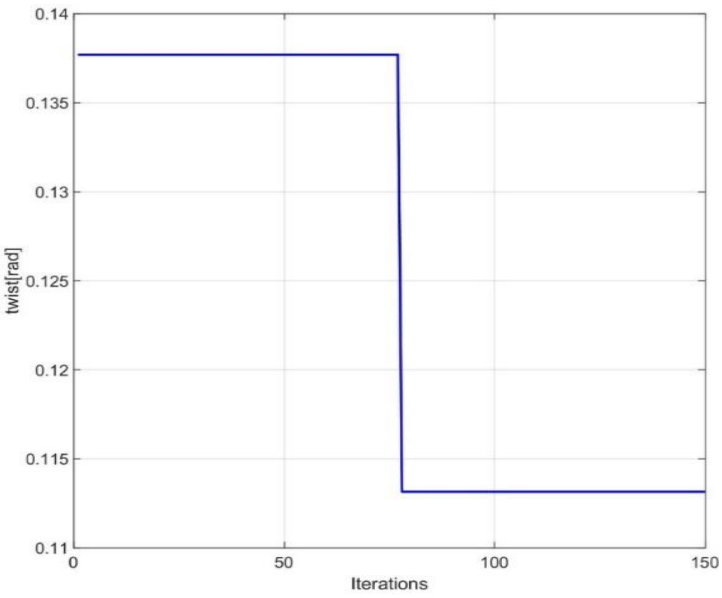

Figure 17: Convergence of the twist for the eighth control point

As can be observed, the optimal solution can be found after the 10th, 20th, or 75th iteration.

3.4. Comparison of the two blade models

Figures 18 and 19 show the evolution of the chord and twist of the baseline blade and the proposed blade. It is observed that for radii less than 4 m, the proposed blade has a larger chord than the baseline blade, whereas for larger radii, the opposite is true (Figure 18).

Regarding the twist angle (Figure 19), at small radii—between 1.5 m and 3 m—the twist of the proposed blade is greater than that of the baseline. Between 3 m and 4 m, both blades have the same twist, and for larger radii, the twist of the baseline blade becomes greater.

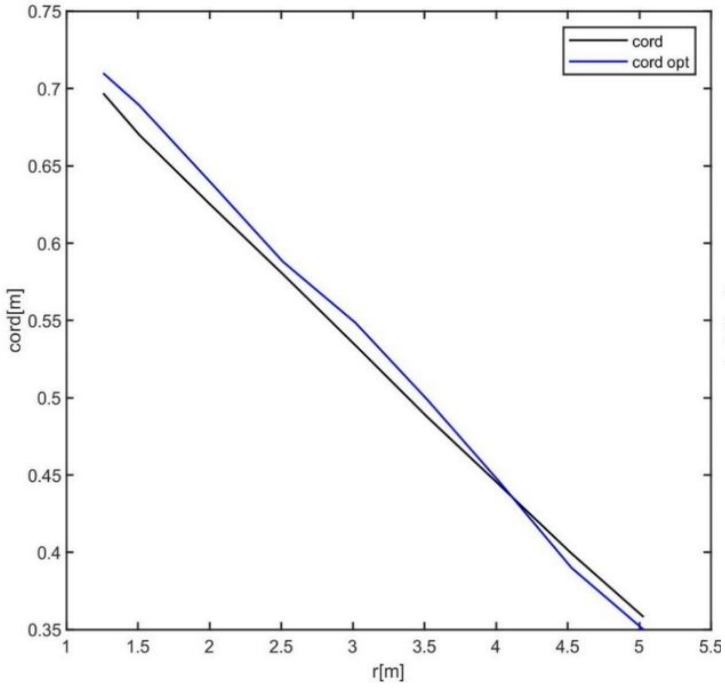

Figure 18: Evolution of the chord of the base blade and the optimized one according to the radius

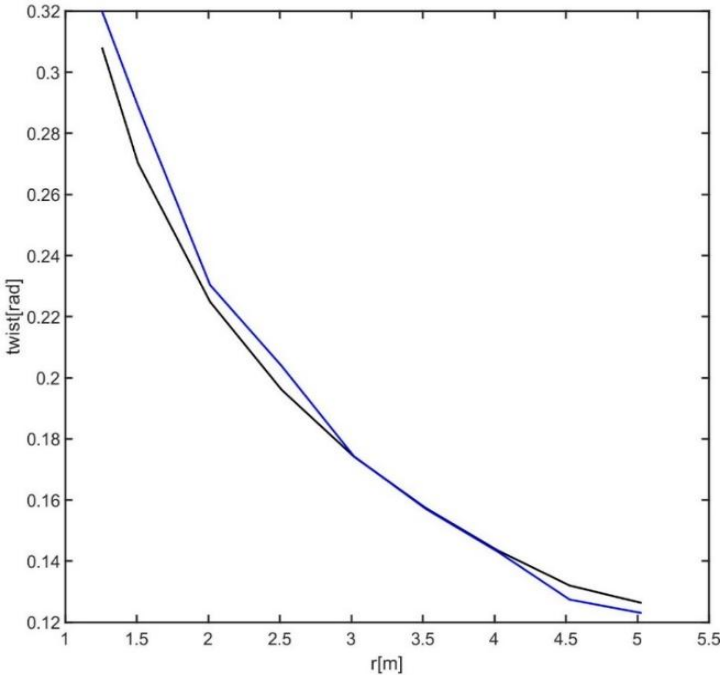

Figure 19: Evolution of the twist of the base blade and the optimized one according to the radius

The evolution of noise level for the two blades models is presented in Figure 20. In the root zone, the proposed blade produces a higher noise level compared to the base blade. This is justified by the fact that it has a thicker chord in this zone. For radii ranging from 2.2 m to 4.5 m the two noises are almost the same, in fact the chord of the proposed blade decreases with the radius. In the tip zone the noise emitted by the proposed blade is slightly below that emitted by the base blade. This is because the proposed blade has a thicker chord in this zone.

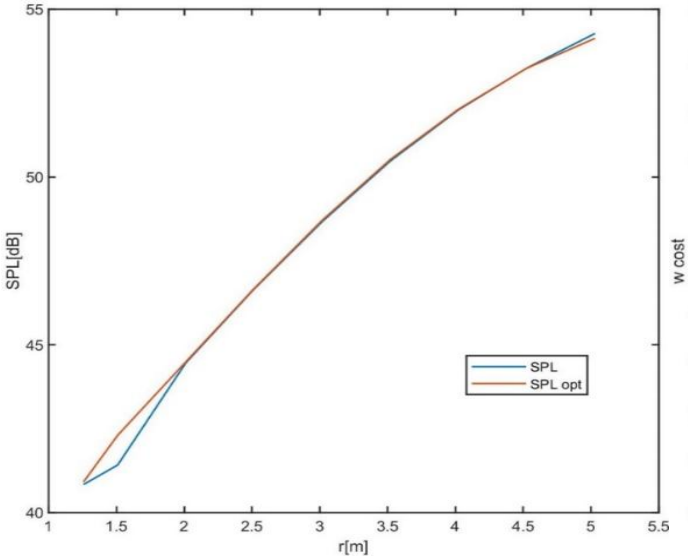

Figure 20: Evolution of the noise of the basic blade and the optimized one

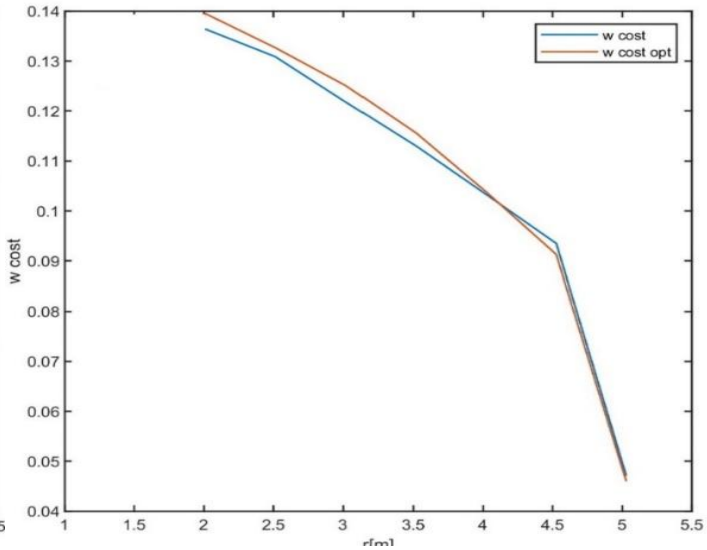

Figure 21: Evolution of the cost of the basic blade and the optimized one

Figure 21 shows the evolution of the cost with respect to the radius for the two blade models. From 2 m to 4 m, the proposed blade has a higher production cost than the baseline blade. This is because the cost depends on the chord length, and in this region, the proposed blade has a wider chord. From 4 m to approximately 4.5 m, the baseline blade has a slightly higher cost than the proposed blade, and from 4.5 m to 5 m, the costs of both blades converge.

Table 6 provides a comparison of power, cost, and total noise level for the two blade models. At 10 m/s, the baseline blade generates a power output of 10.91 kW, while the new blade produces 11.242 kW, representing a 3% increase. The cost rises from 1 to 1.012, indicating a 1.2% increase, and the noise level decreases from 58.178 dB to 58.1555 dB, a reduction of 0.04%. This reduction is beneficial for residents near wind farms, as a 0.04 dB reduction per blade can translate into a reduction of 4 dB or more at the wind farm level, depending on the number of turbines. In summary, the proposed blade delivers more energy while slightly reducing the noise level, albeit with a modest increase in production cost.

Table 6: Summary

	Basic_blade	Optimum_blade	Gain percentage (%)
Power (Kw)	10,91	11,242	3,04
Cost (-)	1	1,012	-1,2
Noise (dB)	58,178	58,1555	0,04

In order to highlight the importance of this new blade model, the blade was simulated under the same experimental conditions as the baseline blade (Figure 22). Additionally, an economic analysis was conducted to estimate the cost per kWh, using the administrative building of the IUT of Ngaoundéré as a reference site. The data related to this site are provided by the work of Kazet [27], particularly the scale parameter *c'* and the form factor *k*. Figure 22 shows the evolution of power as a function of wind speed for the different rotors. For low wind speeds,

ranging from 5 to 8 m/s, the two curves are nearly identical. However, at higher wind speeds, the power generated by the optimized rotor exceeds that of the baseline rotor.

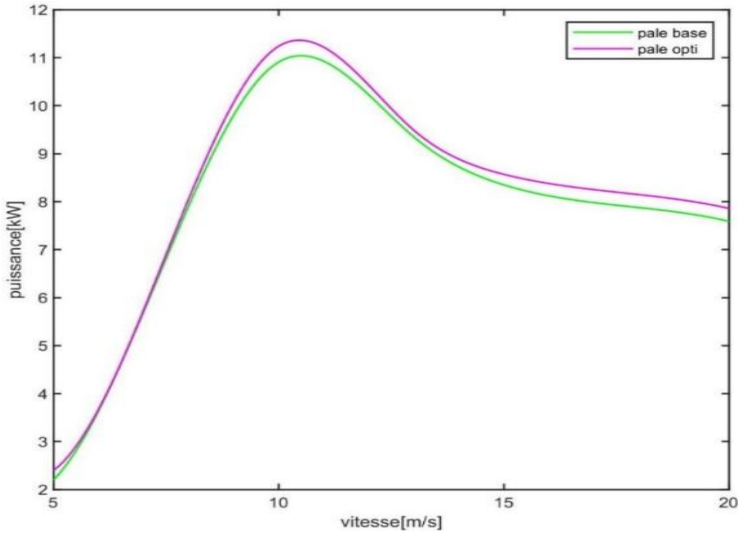

Figure 22: Evolution of the power supplied by the basic blade and the optimized one as a function of speeds

This shows that the proposed blade can be used for both low and high wind speeds, and it is more efficient at high wind speeds.

The annual energy produced by the two rotors was estimated, assuming they are installed at the site (IUT of Ngaoundere). The energy output increased from 27.3 to 29.587 kWh, representing a gain of approximately 2.2 kWh.

The price per kilowatt-hour was also evaluated, as shown in Table 7, using the same installation site. It decreased from 0.0728 to 0.068, representing a 6.6% reduction in kWh cost. Thus, although the increase in production cost requires additional investment from the company, the 6.6% reduction in kWh price makes the blade highly attractive to consumers.

Table 7: Price per kWh

	Basic_blade	Optimum_blade
Production cost ($)	2 200	2 226
PCV($)	$1{,}988 \times 10^3$	$2{,}012 \times 10^3$
AEP (Kwh)	27,3	29,587
Price per kWh ($)	0,0728	0,068

4. Conclusion

In this study, a new blade model was proposed through a multi-objective optimization using the PSO algorithm. This optimization was based on three objective functions: increasing aerodynamic performance (particularly power), reducing production cost, and minimizing aerodynamic noise. The design variables considered were the twist and chord distributions along the blade span. Aerodynamic performance was evaluated using the modified prescribed wake method proposed by Choupo, noise was assessed using Brooks' empirical method, and cost was

calculated using Xudong's method. Nine control points were selected along the blade, and optimization was performed point by point. The proposed blade model features a thicker chord at the root and a more refined chord at the tip compared to the baseline model. The twist angle is also larger at the root and decreases toward the tip. The new blade model enables a 3% increase in power output, a 1.2% increase in production cost, and a 6.6% reduction in the price of energy. This blade can be particularly useful for regions like Ngaoundéré and elsewhere where energy demand is increasing.

Financial supports

No funds, grants or other financial support was received to conduct this study or to prepare the manuscript.

Competing interests

The authors declare that they have no known competing financial interests or personal relationships that could have appeared to influence the work reported in this paper.

Acknowledgements.

The authors appreciatively acknowledge the chief of the Biochemical and Alimental Technologic Laboratory of the University of Ngaoundere as well as the various heads of the Doctoral Training Unit of Engineering Sciences, the Doctoral School of Fundamental and Applied Sciences of the University of Douala and Mr. Fotsop Cyrille Ghislain of the Institute of Chemistry, Faculty of Process and Systems Engineering, Universität Splatz 2, 39106 Magdeburg Germany for his availability for the characterization of biomasses.

References

[1] Snel, H. (2003). Review of aerodynamics for wind turbines. *Wind Energy*, *6*(3), 203–211. https://doi.org/10.1002/we.97.

[2] Clifton-Smith, M. J., & Wood, D. H. (2007). Further dual purpose evolutionary optimization of small wind turbine blades. *Journal of Physics: Conference Series*, *75*, 012017. IOP Publishing. https://doi.org/10.1088/1742-6596/75/1/012017.

[3] Perfiliev, D., Hämäläinen, J., & Backman, J. (2013). Robust analyzing tools for wind turbine blades coupled with multi-objective optimization. *Journal of Energy and Power Engineering*, *7*(10), 1831.

[4] Polat, Ö., & Tuncer, İ. H. (2013). Aerodynamic shape optimization of wind turbine blades using a parallel genetic algorithm. *Procedia Engineering*, *61*, 28–31. https://doi.org/10.1016/j.proeng.2013.07.088

[5] Hassanzadeh, A., Hassanabad, A. H., & Dadvand, A. (2016). Aerodynamic shape optimization and analysis of small wind turbine blades employing the Viterna approach for the post-stall region. *Alexandria Engineering Journal*, *55*(3), 2035–2043. https://doi.org/10.1016/j.aej.2016.07.008.

[6] Timmer, W. (2013). Aerodynamic characteristics of wind turbine blade airfoils. In P. Brønsted & R. Nijssen (Eds.), *Advances in wind turbine blade design and materials*. Woodhead Publishing.

[7] Chehouri, A., Younes, R., Ilinca, A., & Perron, J. (2015). Review of performance optimization techniques applied to wind turbines. *Applied Energy*, *142*, 361–388. https://doi.org/10.1016/j.apenergy.2014.12.043.

[8] Chkir, S., Dobrev, I., Kuszla, P., & Massouh, F. (2009). Unsteady loads evaluation for a wind turbine rotor. *Diagnostyka*, *50*, 17–22.

[9] Derakhshan, S., & Tavaziani, A. (2015). Study of wind turbine aerodynamic performance using numerical methods. *Journal of Clean Energy Technologies*, *3*(2), 83–90. https://doi.org/10.7763/JOCET.2015.V3.174.

[10] Maalouf, C. B. (2010). *Étude des phénomènes tourbillonnaires dans le sillage éolien* (Doctoral dissertation, Université Arts et Métiers ParisTech, France). 149 pp.

[11] Xu, B., Feng, J., Wang, T., Yuan, Y., & Zhao, Z. (2018a). Application of a turbulent vortex core model in the free vortex wake scheme to predict wind turbine aerodynamics. *Journal of Renewable and Sustainable Energy, 10*(2), 023303. https://doi.org/10.1063/1.5020200

[12] Meghlaoui, I. (2018). *Contribution à l'étude d'une chaîne de conversion éolienne de faible puissance à axe horizontal* (Thèse de doctorat, Université de Badji Mokhtar-Annaba, Algérie). 93 pages.

[13] Dumitrescu, H., & Cardos, V. (1998). Wind turbine aerodynamic performance by lifting line method. *International Journal of Rotating Machinery, 4*(3), 141–149.

[14] Currin, H. D., Coton, F. N., & Wood, B. (2008). Dynamic prescribed vortex wake model for AERODYN/FAST. *Journal of Solar Energy Engineering, 130*(3), 031011. https://doi.org/10.1115/1.2931503

[15] Burton, T., Jenkins, N., Sharpe, D., & Bossanyi, E. (2011). *Wind energy handbook* (2nd ed.). John Wiley & Sons.

[16] Yuego, C., Tientcheu Nsiewe, M., Matuam Tamdem, B., Gnepie-Takam, N., & Kuitche, A. (2023). Development of a new aerodynamic method for the mechanical characterization of a horizontal axis wind turbine. *Applied Engineering, 7*(2), 37–46. https://doi.org/10.11648/j.ae.20230702.12

[17] Brooks, T. F., Pope, D. S., & Marcolini, M. A. (1989). *Airfoil self-noise and prediction* (NASA Reference Publication No. 1218). National Aeronautics and Space Administration.

[18] Xudong, W., Shen, W. Z., Zhu, W. J., Sørensen, J. N., & Jin, C. (2009). Shape optimization of wind turbine blades. *Wind Energy, 12*(8), 781–803. https://doi.org/10.1002/we.335

[19] Lindenburg, C. (2003). *Investigation into rotor blade aerodynamics: Analysis of the stationary measurements on the UAE phase-VI rotor in the NASA-Ames wind tunnel* (ECN Report No. ECN-C--03-025). Energy Research Centre of the Netherlands (ECN).

[20] Eberhart, R. C., & Kennedy, J. (1995). A new optimizer using particle swarm theory. In *Proceedings of the Sixth International Symposium on Micro Machine and Human Science* (pp. 39–43). IEEE. https://doi.org/10.1109/MHS.1995.494215

[21] Kendeg Onla, J. C., Guidkaya, G., Kenmoe Fankem, E. D., Dountio Tchioffo, A., & Effa, J. Y. (2024). Reluctance network modeling and optimization of brushless doubly-fed machines for wind power generation. *Insight: Electrical and Electronic Engineering, 1*(1), 1–11.

[22] Salau, Y. W., Gebru, W., & Bitew, D. (2020). Optimal network reconfiguration for power loss minimization and voltage profile enhancement in distribution systems. *Heliyon, 6*(6), e04233. https://doi.org/10.1016/j.heliyon.2020.e04233

[23] Eke, G., & Onyewudiala, J. (2010). Optimization of wind turbine blades using genetic algorithm. *Global Journal of Researches in Engineering, 10*(7).

[24] Lowson, M. V. (1993). A new prediction model for wind turbine noise. In *Proceedings of the Renewable Energy Conference* (pp. 17–19). IEE, London.

[25] Mathew, S. (2006). *Wind energy: Fundamentals, resource analysis and economics*. Springer Science & Business Media. https://doi.org/10.1007/3-540-30906-3

[26] Gökçek, M., & Genç, M. S. (2009). Evaluation of electricity generation and energy cost of wind energy conversion systems (WECSs) in central Turkey. *Applied Energy, 86*(12), 2731–2739. https://doi.org/10.1016/j.apenergy.2009.03.025

[27] Kazet, M., Mouangue, R., Kuitche, A., Ndjaka, J. M., & Takam, S. (2013). Modélisation et simulation numérique des données du vent en vue d'une prédiction de l'énergie électrique d'origine éolienne : Cas d'un site de la ville de Ngaoundéré au Cameroun. *Journal of Renewable Energies, 16*(3), 527–538. https://doi.org/10.54966/jreen.v16i3.397